Phonon-limited carrier mobility and temperature-dependent scattering mechanism of 3C-SiC from first principles

Fanchen Meng, Jinlong Ma, Jian He, and Wu Li

Phys. Rev. B **99**, 045201 — Published 28 January 2019

DOI: 10.1103/PhysRevB.99.045201

Phonon-limited carrier mobility and temperature-dependent scattering mechanism of 3C-SiC from first principles

Fanchen Meng,[1] Jinlong Ma,[2] Jian He,[1] and Wu Li[2,*]

[1] *Department of Physics and Astronomy, Clemson University, Clemson 29634, USA*
[2] *Institute for Advanced Study, Shenzhen University, Shenzhen 518060, China*

Electron-phonon coupling is at the core of various regimes of material-based science and technology. Taking 3C-silicon carbide (3C-SiC) as an example, despite its very wide application in high temperature and high power devices, the transport properties of 3C-SiC are not yet fully understood at the microscopic level because of inadequate knowledge in electron-phonon coupling. In this work, with electron-phonon coupling matrix elements calculated from first principles, the phonon limited carrier mobility of 3C-SiC is quantified by solving the Boltzmann transport equation. The calculated mobilities for both holes and electrons are in reasonable agreement with the experimental data. Unlike other polar semiconductors such as GaAs, where the polar-longitudinal-optical-phonon interactions are the dominant scattering mechanism, the mobilities of electrons and holes are dominated by the intravalley longitudinal acoustic (LA) phonon scattering at $300K$ due to the low occupation number of high-frequency polar longitudinal optical (LO) phonons in 3C-SiC. The dominant scattering mechanism in 3C-SiC varies with temperature. At high temperature ($800K$), LO phonons govern the scattering instead. The maximum mean free paths of electrons and holes at room temperature are found to be 40 nm and 15 nm, respectively.

I. INTRODUCTION

Silicon carbide (SiC) is one of the most promising alternatives to silicon for high temperature and/or high power devices because of its unique combination of wide band gap[1,2], high breakdown voltage[1,2], and high thermal conductivity[3–5]. The performance of SiC-based devices has been demonstrated in past decades[6–12]. From a fundamental research point of view, SiC is interesting in its own right. For example, SiC has numerous allotropes, among which the cubic phase (3C) and hexagonal phases (4H and 6H) are the most interesting. Note that the device applications of SiC rely on its electrical transport properties. Concerning the electrical transport properties, the 4H and 3C phases have been reported to have substantially higher electron mobility than the 6H phase[13]. In particular, 3C-SiC adopts a simple zincblende crystal structure, which is isotropic, with several advantages compared to other allotropes with respect to applications.

Despite the abundance data in literature, both experimental[14–17] and theoretical[18–26], the electrical transport properties of 3C-SiC have not yet been fully understood at the microscopic level. The experimental electron mobilities vary greatly from sample to sample, intimately related to the quality and growth conditions. For example, Nelson *et al.*[17] reported a room temperature electron mobility of 890 $cm^2/V{\cdot}s$ in single crystalline 3C-SiC. Shinohara *et al.*[14] obtained a value larger than 750 $cm^2/V{\cdot}s$ in undoped 3C-SiC epitaxial film grown on carbonized silicon surfaces. Yamanaka *et al.*[16] obtained a much smaller value $\sim$ 500 $cm^2/V{\cdot}s$ for unintentionally doped n-type 3C-SiC layers epitaxially grown on silicon, and the authors argued that longitudinal acoustic (LA) phonons dominate the scattering mechanism at room temperature and above. On the theory side, a value of 1300 $cm^2/V{\cdot}s$ at $300K$ has been reported which assumes polar longitudinal optical (LO) phonon scattering being the dominant scattering mechanism[26]. These early studies focused mainly on n-type 3C-SiC, however, the research on p-type 3C-SiC is scarce. Thus, there is a knowledge gap regarding p-type 3C-SiC, preventing us from obtaining a coherent and complete picture of the electrical transport properties of 3C-SiC.

As discussed above, electron-phonon coupling is at the core of understanding the electrical transport properties of 3C-SiC at the microscopic level. To this end, first principles calculations of carrier transport properties are the tool of choice to fill this gap of knowledge. However, first principles calculations of carrier transport properties are computationally expensive as very dense meshes of Brillouin zone sampling are required for both carriers and phonons. The lately developed interpolation methods for electron-phonon coupling matrix elements[27–31] greatly reduced the time required for calculating the electron-phonon coupling matrix elements. The efficiency of these methods has been confirmed in both nonpolar materials and polar materials[28,32–38]. Therefore, in this work, we carry out first principles calculations to have a deeper understanding of the intrinsic electron and hole transport mechanism of single crystalline 3C-SiC. In particular, the Wannier function interpolation method[27,29–31] is employed to obtain the electron-phonon coupling matrix elements, which are then used to calculate phonon-limited scattering rates and carrier mobilities by solving the Boltzmann transport equation (BTE).

II. METHODOLOGY

If there is an external electric field $\mathbf{E}$, the electron distribution function $f_{n\mathbf{k}}$ of the $n\mathbf{k}$ state, with band index n and wave vector $\mathbf{k}$, will deviate from its equilibrium

Fermi-Dirac distribution $f^0_{n\mathbf{k}}$. By solving BTE[39], we are able to obtain the electron distribution function, $f_{n\mathbf{k}}$, which will be affected by both the electric field $\mathbf{E}$ and the allowed scattering processes, leading the system to a steady state, where the BTE is expressed as[28]

$$-\frac{q\mathbf{E}}{\hbar}\frac{\partial f_{n\mathbf{k}}}{\partial \mathbf{k}} + \frac{\partial f_{n\mathbf{k}}}{\partial t}|_{\text{scatt}} = 0, \tag{1}$$

where q is elementary charge and $\hbar$ is the reduced Planck constant. If the external electric field $\mathbf{E}$ is small enough, $f_{n\mathbf{k}}$ could be expressed using Taylor expansion as $f_{n\mathbf{k}} = f^0_{n\mathbf{k}} + f_{n\mathbf{k}}(1 - f_{n\mathbf{k}})\phi_{n\mathbf{k}}$, with $\phi_{n\mathbf{k}}$ being a small perturbation which is linear with respect to $\mathbf{E}$. Therefore, it is convenient to express $\phi_{n\mathbf{k}}$ as $\frac{q\mathbf{E}}{k_\mathrm{B}T}\cdot\mathbf{F}_{n\mathbf{k}}$, with k_B being the Boltzmann constant, T being the temperature. $\mathbf{F}_{n\mathbf{k}}$ can be considered as the mean free displacement[28,40]. If the scattering term (second term) of Equation (1) is limited to the electron-phonon coupling, Equation (1) can be linearized:[28]

$$\mathbf{F}_{n\mathbf{k}} = \mathbf{v}_{n\mathbf{k}}\tau^0_{n\mathbf{k}} + \tau^0_{n\mathbf{k}}\sum_{\mathbf{q}pm}(\Gamma^{m\mathbf{k}+\mathbf{q}}_{n\mathbf{k},\mathbf{q}p} + \Gamma^{m\mathbf{k}+\mathbf{q},-\mathbf{q}p}_{n\mathbf{k}})\mathbf{F}_{m\mathbf{k}+\mathbf{q}}, \tag{2}$$

where $\mathbf{q}p$ represents the phonon mode with branch p and wave vector $\mathbf{q}$, $\mathbf{v}_{n\mathbf{k}}$ describes the group velocity of carrier defined as $\mathbf{v}_{n\mathbf{k}} = \frac{1}{\hbar}\frac{\partial \mathbf{E}_{n\mathbf{k}}}{\partial \mathbf{k}}$, and $\tau^0_{n\mathbf{k}}$ is the relaxation time which could be calculated as $[\sum_{\mathbf{q}pm}(\Gamma^{m\mathbf{k}+\mathbf{q}}_{n\mathbf{k},\mathbf{q}p} + \Gamma^{m\mathbf{k}+\mathbf{q},-\mathbf{q}p}_{n\mathbf{k}})]^{-1}$. Here, $\Gamma^{m\mathbf{k}+\mathbf{q}}_{n\mathbf{k},\mathbf{q}p}$ and $\Gamma^{m\mathbf{k}+\mathbf{q},-\mathbf{q}p}_{n\mathbf{k}}$ are transition rates for phonon absorption and emission processes, respectively[28], which can be obtained from electron-phonon coupling strength calculated via first principles method as

$$\Gamma^{m\mathbf{k}+\mathbf{q}}_{n\mathbf{k},\mathbf{q}p} = \frac{2\pi}{\hbar}|g^{m\mathbf{k}+\mathbf{q}}_{n\mathbf{k},\mathbf{q}p}|^2(f^0_{\mathbf{k}+\mathbf{q}} + N^0_{\mathbf{q}p}) \times\delta(E_{n\mathbf{k}} + \hbar\omega_{\mathbf{q}p} - E_{m\mathbf{k}+\mathbf{q}}), \tag{3}$$

$$\Gamma^{m\mathbf{k}+\mathbf{q},-\mathbf{q}p}_{n\mathbf{k}} = \frac{2\pi}{\hbar}|g^{m\mathbf{k}+\mathbf{q}}_{n\mathbf{k},\mathbf{q}p}|^2(1 + N^0_{-\mathbf{q}p} - f^0_{m\mathbf{k}+\mathbf{q}}) \times\delta(E_{n\mathbf{k}} - \hbar\omega_{-\mathbf{q}p} - E_{m\mathbf{k}+\mathbf{q}}), \tag{4}$$

where $g^{m\mathbf{k}+\mathbf{q}}_{n\mathbf{k},\mathbf{q}p}$ is the electron-phonon coupling matrix element, $N^0_{\mathbf{q}p}$ is the Bose-Einstein distribution function for phonons and the δ function guarantees the conservation of energy and momentum during the scattering process.

Equation (2) can be solved iteratively to find $\mathbf{F}_{n\mathbf{k}}$, which is also called the exact solution. This method has been applied to studying phonon transport properties[40–42] for a few years, but has not been introduced to the study of electron transport properties until very recently[28,33–35,37,38]. For the exact solution to $\mathbf{F}_{n\mathbf{k}}$, the $\mathbf{k}$ and $\mathbf{q}$ grids are required to be commensurate[27,31]. Besides the exact solution, for comparison, two more solutions are also implemented in our calculation, which are conventional relaxation time approximation (conventional-RTA) method and momentum relaxation time approximation (momentum-RTA) method. Conventional-RTA neglects the sum term (second term) on the right-hand side of Equation (2). Momentum-RTA also neglects this sum and further takes account for the relative change of momentum in each scattering process by multiplying the transition rates involved in $\tau^0_{n\mathbf{k}}$ by an efficiency factor of[28]

$$\lambda = 1 - \frac{\mathbf{v}_{n\mathbf{k}}\cdot\mathbf{v}_{m\mathbf{k}+\mathbf{q}}}{|\mathbf{v}_{n\mathbf{k}}|^2}. \tag{5}$$

At a finite temperature T, with the calculated $\mathbf{F}_{n\mathbf{k}}$, the electrical conductivity tensor can be expressed as

$$\sigma^{\alpha\beta} = \frac{2q^2}{NVk_\mathrm{B}T}\sum_{n\mathbf{k}} f^0_{n\mathbf{k}}(1 - f^0_{n\mathbf{k}})v^\alpha_{n\mathbf{k}}F^\beta_{n\mathbf{k}}, \tag{6}$$

where N is the number of $\mathbf{k}$ meshes, V is the volume of the unit cell, α and β are Cartesian directions. For example $v^\alpha_{n\mathbf{k}}$ is electron velocity along α direction. For high-symmetry systems such as 3C-SiC studied in this work with space group $F\bar{4}3m$, the electrical conductivity tensor $\sigma^{\alpha\beta}$ is reduced to a scalar σ, from which mobility can be obtained as

$$\mu = \frac{\sigma}{n_c q}, \tag{7}$$

where n_c is carrier density. For n-type, $n_c = \frac{2}{NV}\sum_{n\mathbf{k}} f^0_{n\mathbf{k}}$, while for p-type $n_c = \frac{2}{NV}\sum_{n\mathbf{k}}(1 - f^0_{n\mathbf{k}})$.

Density functional theory (DFT) is employed to calculate the geometric structure and electronic band structure, while density functional perturbation theory (DFPT) is used to obtain phonon dispersion relation and initial electron-phonon coupling matrix elements as implemented in QUANTUM ESPRESSO package[43] with norm-conserving pseudopotential under the local density approximation (LDA)[44]. The plane-wave cutoff energy is set to be 58 Ry, and $16\times16\times16$ Monkhorst-Pack k meshes are used for structure relaxation, both of which are well converged. The lattice structure of 3C-SiC is shown in Fig. 1(a) with the relaxed lattice constant of 4.326 Å, agreeing well with experimental value 4.360 Å[45]. To interpolate the electron-phonon coupling matrix elements, the EPW package[31] is employed to perform Wannier function interpolation. The initial coarse grids are chosen as $6\times6\times6$ for both $\mathbf{k}$ and $\mathbf{q}$. The chemical potential is manually chosen to be 0.3 eV in the band gap away from the band edges, to ensure that the calculated mobility is intrinsically phonon-limited and corresponds to a low carrier concentration limit, where the defect scattering can be ignored.

III. RESULTS AND DISCUSSION

It has been reported that the spin orbit coupling (SOC) effect, which leads to the splitting of the degenerate valence band, has a great influence on the hole mobility in different materials[34,37,38]. Therefore in our calculation, SOC is included for the calculation of electronic band structure, phonon dispersion relation, and

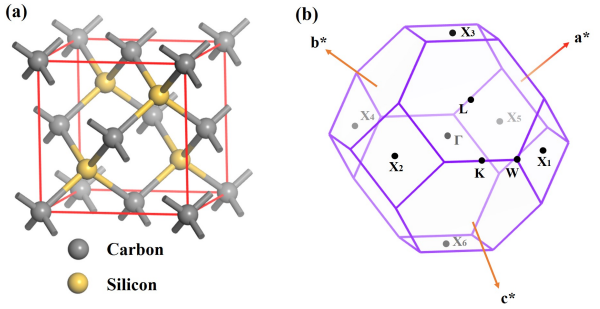

FIG 1. (Color online) (a) Geometric structure of 3C-SiC (conventional unit cell) and (b) first Brillouin zone of 3C-SiC with the high symmetry points labeled. The fractional coordinates for the high symmetry points with respect to reciprocal lattice vectors are: X_1=(0.5, 0, 0.5), X_2=(0, 0.5, 0.5), X_3=(0.5, 0.5, 0), X_4=(-0.5, 0, -0.5), X_5=(0, -0.5, -0.5), X_6=(-0.5, -0.5, 0), K=(0.375, 0.375, 0.75), W=(0.5, 0.25, 0.75) and L=(0.5, 0.5, 0.5).

electron-phonon coupling matrix elements unless otherwise stated. The electronic band structure along high-symmetry paths [Fig. 1(b)] is shown in Figure 2(a). 3C-SiC has an indirect band gap, with the valence band maximum (VBM) located at Γ point, and the conduction band minimum (CBM) sitting at X point. The calculated band gap is 1.34 eV, smaller than the experimental value of 2.42 eV[46]. This is a result of DFT usually underestimating the energy of band gaps. However, the band gap has no effect on the calculated transport properties. With SOC, as can be seen from the inset of Figure 2(a), there is a small split-off energy gap about 15 meV in the valence band, close to the experimental value of 10 meV[47]. The calculated phonon dispersion relation along with experimental data are shown in Figure 2(b). It is clear that the calculated phonon dispersion relation is in excellent agreement with the experimental values from both inelastic X-ray scattering[48] and Raman measurement[49]. It is worth noting here that the highest frequency of the longitudinal optical (LO) phonons is 121 meV, which is larger than those in some common semiconductors such as silicon[34,38] and GaAs[32–34].

The mobility calculation is very time and memory consuming, and it is always necessary to do a convergence test on the **k** and **q** grids. As can be seen in Figure 3, at room temperature, the obtained mobilities of holes and electrons are well converged with the relative difference around 2% when the fine **k** and **q** meshes are both $120 \times 120 \times 120$.

With the converged **k** and **q** meshes mentioned above, the calculated carrier mobilities as a function of temperature are depicted in Figure 4. For both electrons and holes, the mobilities obtained with exact solution to the BTE (labeled as ITER in Figure 4) agree very well with the experimental results in a broad temperature range, from 200K to 600K. However, the conventional-RTA method strongly underestimates the mobilities by more

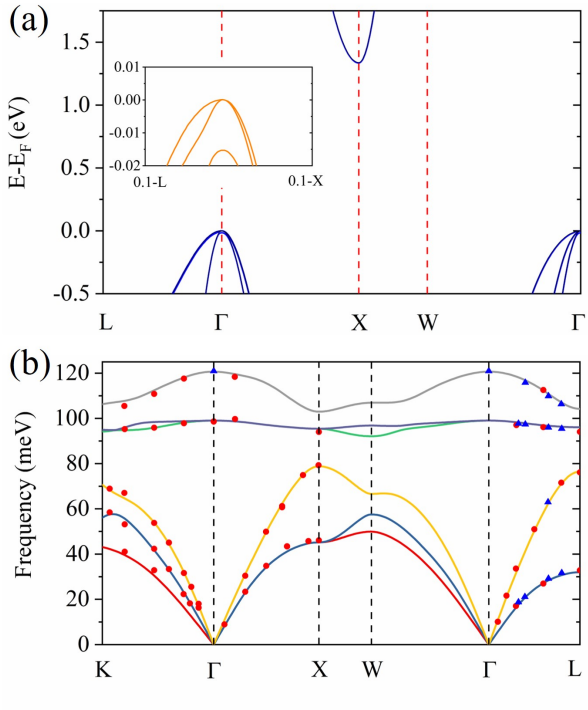

FIG 2. (Color online) (a) Electronic band structure and (b) phonon dispersion relation along high-symmetry points in the first Brillouin zone. Inset: zoom-in of the valence band, where the split-off gap is significantly clearer. Experimental data for phonon dispersion are taken from Ref [49] and Ref [48]. Different branches: transverse acoustic (TA1 and TA2), longitudinal acoustic (LA), transverse optical (TO1 and TO2), and longitudinal optical (LO) are depicted in different colors.

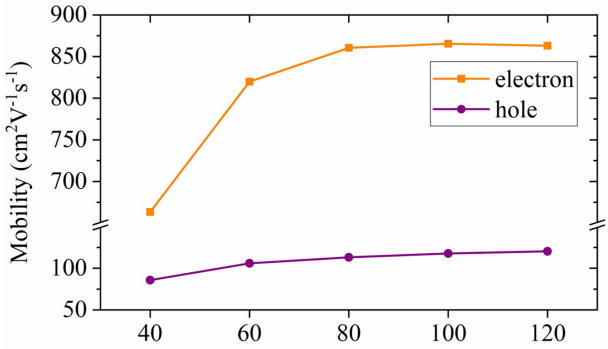

FIG 3. (Color online) Convergence on the carrier mobilities at 300K with respect to **k** and **q** grids. Here, in light of the high symmetrical cubic structure of 3C-SiC, the number n on the horizontal axis represents $n \times n \times n$ **k** and **q** fine grids.

than 31% and 17% variance for electrons and holes, respectively.

Mobilities obtained without SOC are also plotted in Figure 4 for comparison. Since SOC does not affect the conduction bands in 3C-SiC, the electron mobilities calculated with and without SOC are identical. On

the other end, calculation without SOC slightly overestimates the hole mobilities. For example, at $300K$, the mobilities obtained with and without SOC effect are 120.4 and 122.8 $cm^2/V{\cdot}s$, respectively. As temperature increases from $200K$ to $800K$, the variance decreases from 2.0% to 1.0%. The thermal energy increasing with temperature can smear out the split-off gap. Only when the thermal energy is much smaller than the split-off gap, SOC can have appreciable effect. The split-off gap of 15 meV corresponds to a temperature of $174K$. Therefore the SOC effect on the hole mobility in the temperature range (from $200K$ to $800K$) studied in this work is negligible and much smaller than that of silicon[34,38] and GaAs[34], because of much smaller split-off energy gap of 3C-SiC (15 meV) when compared with silicon ($\sim$ 44 meV)[34,50] and GaAs ($\sim$ 330 meV)[34,51,52].

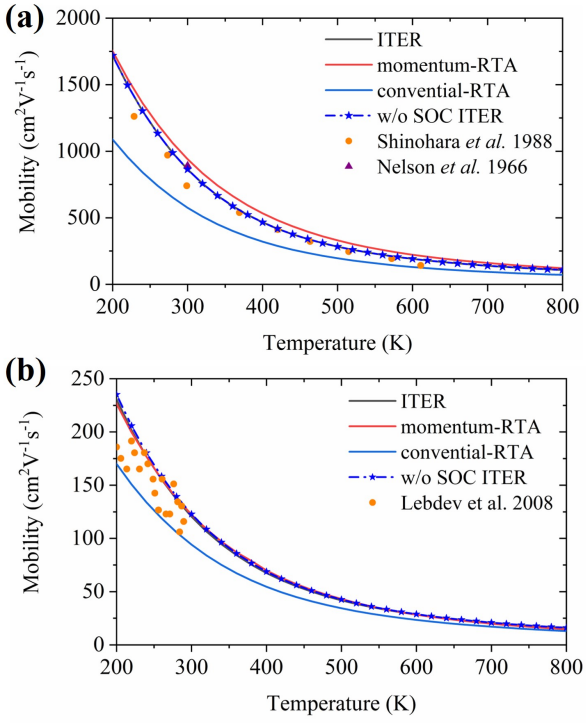

FIG 4. (Color online) Mobilities of electron (a) and hole (b) as a function of temperature. The experimental results for electrons are taken from Ref [14] and Ref [17], and is from Ref [53] for holes. It should be noted that the mobilities obtained by full solution with and without SOC are overlaid on each other in the figure.

Figure 5 shows the scattering rates of electrons and holes decomposed into each phonon mode of 3C-SiC at $300K$. There are two sudden jumps, signifying the onset of emission processes of certain phonon modes. Electrons and holes share a common jump at 121 meV, corresponding to the emission processes of the LO phonon at Γ point. For electrons, the other jump is located at 79 meV, related to the LA phonon at X point. For holes, the other sits at 99 meV which is relevant to the TO

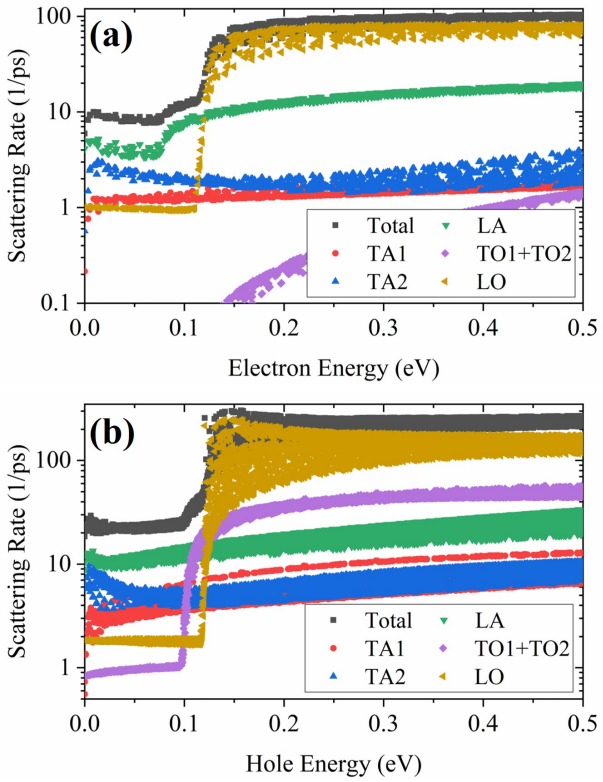

FIG 5. (Color online) Total and decomposed scattering rates of (a) electrons and (b) holes in 3C-SiC at $300K$.

phonon at Γ point.

As can be seen, LA phonons dominate the electron-phonon scatterings for electrons with energy less than 121 meV, which actually contribute 97% to its total mobility. In the case of holes, LA phonons still govern the electron-phonon interactions with hole energy less than 99 meV, from which 93% of the total mobility is reached. This indicates that the LA phonon scattering is the governing scattering mechanism in 3C-SiC at $300K$, in consistent with experimental observation[16,54]. This is, however, in contrast to other polar materials, such as GaAs[33,34], PbTe[55], SnSe[35] and SnTe[36], in which polar LO phonons dominate the scattering for a wide energy range including band edges. Actually, LO-phonon scattering increases suddenly by two orders of magnitude at 121 meV due to the occurrence of phonon emission processes. As a result, LO phonons dominate the scattering above 121 meV. To understand the orders of magnitude smaller scattering below 121 meV for the LO-phonon absorption processes, we refer to Equation (3) and (4). Since the electron/hole occupation number can be neglected in the intrinsic limit, the scattering rates from absorption and emission processes are proportional to $N^0_{\mathbf{q}p}$ and $1+N^0_{-\mathbf{q}p}$, respectively, which is due to the Boson nature of phonons. The LO phonon corresponds to an energy of 121 meV, which is much larger than the thermal energy at $300K$. Therefore, the LO phonon is almost unexcited at room temperature, and $(1+N^0_{\mathbf{\Gamma},\mathrm{LO}})/N^0_{\mathbf{\Gamma},\mathrm{LO}}$ is 105. This also

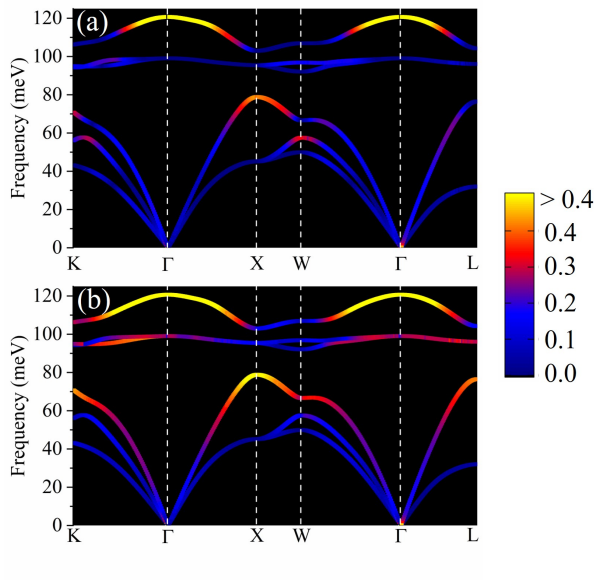

FIG 6. (Color online) Calculated electron-phonon coupling matrix elements $|g^{m\mathbf{k}+\mathbf{q}}_{n\mathbf{k},\mathbf{q}p}|$ (in unit of eV) of (a) initial CBM and (b) initial VBM electron with different phonon branches along high-symmetry directions in the first Brillouin zone.

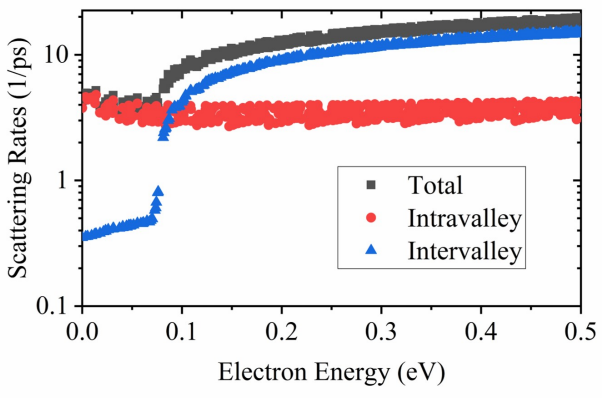

FIG 7. (Color online) Contribution of intravalley and intervalley scattering to LA scattering rates for electrons at the room temperature.

indicates that the large LO phonon frequency typically suggests small scattering. It should be noted that in a very recent paper[37], the authors also mentioned that the frequency of LO phonons are also very high in boron based semiconductors, leading to the suppression of the contribution of LO phonons to the total scattering rates.

Transverse optical (TO) phonon scatterings for holes are larger than those for electrons by more than one order of magnitude. As a result, the signature of the corresponding phonon emission processes is evident in the total scattering rates for holes but not for electrons. To understand this, we plot electron-phonon coupling matrix elements $|g|$ of electrons and holes at band extrema with each phonon branch along high symmetry paths in Figure 6(a) and (b), respectively. Clearly, $|g|$ with TO modes at Γ for holes is much larger than that for electrons. $|g|$ is actually very sensitive to the nature of electronic orbitals. For instance, $|g|$ is found to be weak for coupling between acoustic phonons and non-bonding orbitals.[56] We also note that $|g|$ with LO modes at Γ point for electrons and holes are comparable.

Since the VBM occurs at Γ point, there is no intervalley scattering for holes. However, the CBM is at the X point, and then intervalley scattering with phonon at X point is allowed for electrons. Due to symmetry, there are six equivalent X points, as shown in Figure 1(b). X_1, X_2 and X_3 are identical to X_4, X_5 and X_6 , respectively, up to a certain reciprocal lattice vector. Two non-identical X points can be connected with another X point. For example, $X_2 - X_1 = X_3$. The intervalley scattering processes are facilitated by the large $|g|$ with LA modes at X point. In Fig.7, we quantify the individual contribution from intravalley and intervalley scatterings to the total LA scattering rates for electrons. The intravalley scattering actually dominates up to 79 meV, whereas the intervalley scattering governs above 79 meV. As aforementioned, the sudden jump of the intervalley scattering rates at 79 meV corresponds to the onset of the emission processes of the LA phonon at the X point. Those electrons below 79 meV contribute 82% to the total mobility. Therefore, the mobilities are dominated by the intravalley LA phonon scattering for both electrons and holes at room temperature.

Figure 8 shows the total scattering rates and the contributions from LA and LO phonons for both electrons and holes at different temperatures. The phonon occupation number and consequently the scattering rates increase with temperature. Notably, the relative increase $[n^{T_2}(E)/n^{T_1}(E)]$ in the occupation number of LO phonons is larger than that of LA phonons with increasing temperature. As a result, the LO scattering becomes comparable to the LA scattering near the band edges at $600K$ and turns to be completely dominant at $800K$. This contrasts with the argument made in Ref [16], in which the authors claimed that both electron and hole mobilities are limited by the acoustic phonon scattering above room temperature.

The mode-specific analysis of mean free paths (MPFs) are shown in Figure 9. At room temperature, the largest MFPs of electrons and holes are about 40 nm and 15 nm, respectively. The largest MFPs of both carriers are found be of the energy range from 0.07 eV to 0.1 eV. In this energy range, the electrons contribute about 75%-94% to its total mobility, while holes contribute 71%93% to the total mobility.

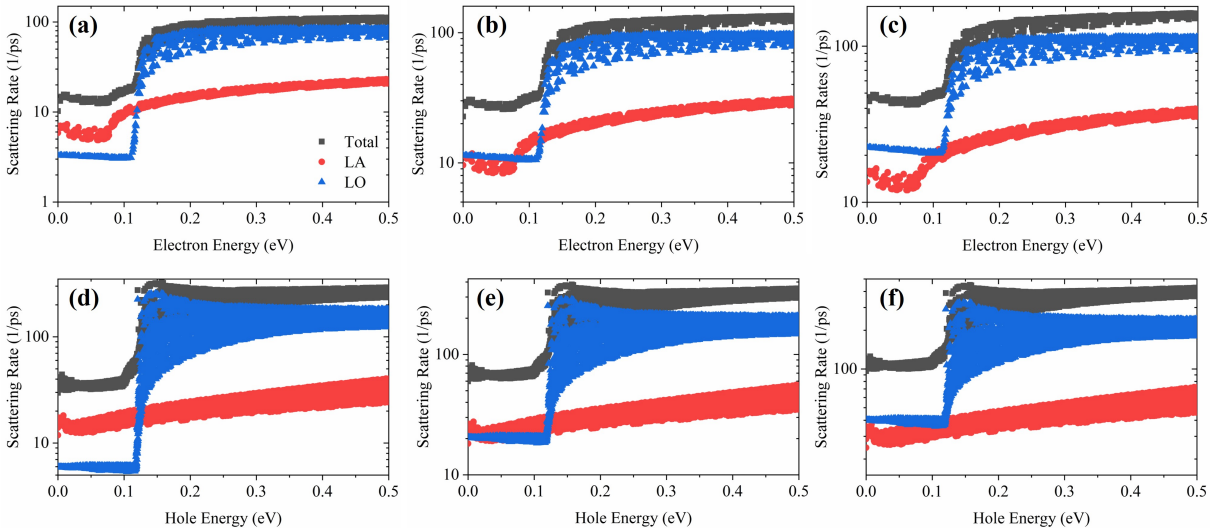

FIG 8. (Color online) Total scattering rates and contributions from LA and LO phonons for electrons at (a) $400K$, (b) $600K$ and (c) $800K$; for holes at (d) $400K$, (e) $600K$ and (f) $800K$

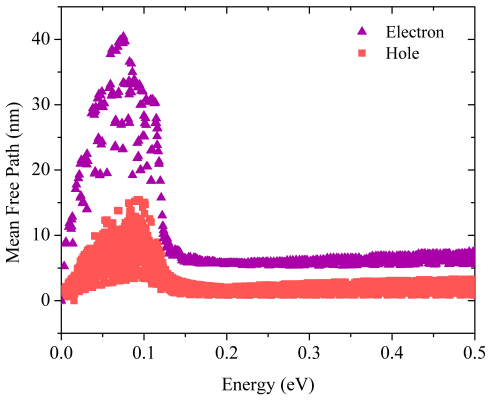

FIG 9. (Color online) Mean free path of (a) electrons and (b) holes in 3C-SiC at $300K$.

IV. CONCLUSIONS

In summary, we performed entire first principles calculations of the mobilities for both n- and p-type 3C-SiC using Boltzmann transport equation (BTE) based on polar Wannier function interpolation of electron-phonon coupling matrix elements. We found a temperature dependent scattering mechanism in 3C-SiC. At room temperature, owing to unexcited longitudinal optical (LO) modes, the longitudinal acoustic (LA) phonons dominate the scatterings of electrons and holes contributing to the mobilities. Specifically, the intravalley LA phonons dominate the scatterings of electrons up to 79 meV, and the intervalley scattering becomes dominant between 79 and 121 meV. The intervalley scattering is not present for holes. At $800K$, LO-phonon interaction becomes the governing scattering mechanism for both electrons and holes. Our calculated mobilities are in good agreement with experimental results. The spin-orbit coupling almost has no influence on the calculated mobilities, especially for the electrons. The largest carrier mean free path is about 40 nm for the electrons and 15 nm for the holes in 3C-SiC at room temperature.

ACKNOWLEDGMENTS

F. Meng and J. He would like to acknowledge the support from NSF DMR 1307740. Especially, F. Meng appreciates the financial support from 2018 ITS Summer Fellowship. J. Ma and W. Li acknowledge the support from the Shenzhen Science, Technology and Innovation Commission under Grant No. JCYJ20170412105922384 and the Natural Science Foundation of China (Grants No. 11704258 and No.11804229). We would like to thank Mr. Myles Mckenna for proof-reading the manuscript. The calculations were performed on the Palmetto high performance cluster, which is managed and maintained by Clemson University CCIT. F. Meng would like to express his special thanks to his dearest mother, Ms. Qingxia Zhang, for her supporting and understanding all her lives.

* wu.li.phys2011@gmail.com

[1] W. Choyke and G. Pensl, Mrs Bulletin **22**, 25 (1997).

[2] L. Patrick, D. Hamilton, and W. Choyke, Physical Review **143**, 526 (1966).
[3] P. G. Neudeck, Journal of Electronic Materials **24**, 283 (1995).
[4] D. Morelli, J. Heremans, C. Beetz, W. Woo, G. Harris, and C. Taylor, in *Institute of Physics Conference Series*, Vol. 137 (Bristol [England]; Boston: Adam Hilger, Ltd., c1985-, 1994) pp. 313–316.
[5] T. Wang, Z. Gui, A. Janotti, C. Ni, and P. Karandikar, Physical Review Materials **1**, 034601 (2017).
[6] F. Yan, J. H. Zhao, and G. H. Olsen, Solid-State Electronics **44**, 341 (2000).
[7] Y. Zhu, J. Zhang, Z. Chen, and T. Egawa, Journal of Applied Physics **106**, 124506 (2009).
[8] K. Schoen, J. M. Woodall, J. A. Cooper, and M. R. Melloch, IEEE Transactions on electron devices **45**, 1595 (1998).
[9] P. Alexandrov, J. Zhao, W. Wright, M. Pan, and M. Weiner, Electronics Letters **37**, 1139 (2001).
[10] P. Ivanov, M. Levinshtein, A. Agarwal, and J. Palmour, Semiconductor science and technology **16**, 521 (2001).
[11] A. K. Agarwal, P. A. Ivanov, M. E. Levinshtein, J. W. Palmour, S. L. Rumyantsev, and S.-H. Ryu, Semiconductor science and technology **16**, 260 (2001).
[12] M. E. Levinshtein, T. T. Mnatsakanov, P. A. Ivanov, A. K. Agarwal, J. W. Palmour, S. L. Rumyantsev, A. G. Tandoev, and S. N. Yurkov, Solid-State Electronics **45**, 453 (2001).
[13] M. Bhatnagar and B. J. Baliga, IEEE Transactions on electron devices **40**, 645 (1993).
[14] M. Shinohara, M. Yamanaka, H. Daimon, E. Sakuma, H. Okumura, S. Misawa, K. Endo, and S. Yoshida, Japanese journal of applied physics **27**, L434 (1988).
[15] T. Tachibana, H. Kong, Y. Wang, and R. Davis, Journal of applied physics **67**, 6375 (1990).
[16] M. Yamanaka, H. Daimon, E. Sakuma, S. Misawa, and S. Yoshida, Journal of applied physics **61**, 599 (1987).
[17] W. Nelson, F. Halden, and A. Rosengreen, Journal of Applied Physics **37**, 333 (1966).
[18] T. Mnatsakanov, L. Pomortseva, and S. Yurkov, Semiconductors **35**, 394 (2001).
[19] H.-E. Nilsson, U. Englund, M. Hjelm, E. Bellotti, and K. Brennan, Journal of applied physics **93**, 3389 (2003).
[20] M. Roschke and F. Schwierz, IEEE Transactions on Electron Devices **48**, 1442 (2001).
[21] T. Mnatsakanov, M. Levinshtein, L. Pomortseva, and S. Yurkov, Semiconductor Science and Technology **17**, 974 (2002).
[22] K. Tsukioka, D. Vasileska, and D. Ferry, Physica B: Condensed Matter **185**, 466 (1993).
[23] R. Joshi and D. Ferry, Solid-State Electronics **38**, 1911 (1995).
[24] R. Mickevičius and J. H. Zhao, Journal of applied physics **83**, 3161 (1998).
[25] E. Bellotti, H.-E. Nilsson, K. F. Brennan, and P. P. Ruden, Journal of applied physics **85**, 3211 (1999).
[26] H. J. Van Daal, *Mobility of charge carriers in silicon carbide* (Philips Research Laboratories, 1965).
[27] J. Noffsinger, F. Giustino, B. D. Malone, C.-H. Park, S. G. Louie, and M. L. Cohen, Computer Physics Communications **181**, 2140 (2010).
[28] W. Li, Physical Review B **92**, 075405 (2015).
[29] C. Verdi and F. Giustino, Physical review letters **115**, 176401 (2015).
[30] J. Sjakste, N. Vast, M. Calandra, and F. Mauri, Phys. Rev. B **92**, 054307 (2015).
[31] S. Poncé, E. R. Margine, C. Verdi, and F. Giustino, Computer Physics Communications **209**, 116 (2016).
[32] J.-J. Zhou and M. Bernardi, Physical Review B **94**, 201201 (2016).
[33] T.-H. Liu, J. Zhou, B. Liao, D. J. Singh, and G. Chen, Physical Review B **95**, 075206 (2017).
[34] J. Ma, A. S. Nissimagoudar, and W. Li, Physical Review B **97**, 045201 (2018).
[35] J. Ma, Y. Chen, and W. Li, Physical Review B **97**, 205207 (2018).
[36] T.-H. Liu, J. Zhou, M. Li, Z. Ding, Q. Song, B. Liao, L. Fu, and G. Chen, Proceedings of the National Academy of Sciences , 201715477 (2018).
[37] T.-H. Liu, B. Song, L. Meroueh, Z. Ding, Q. Song, J. Zhou, M. Li, and G. Chen, Phys. Rev. B **98**, 081203 (2018).
[38] S. Poncé, E. R. Margine, and F. Giustino, Physical Review B **97**, 121201 (2018).
[39] J. M. Ziman, *Electrons and phonons: the theory of transport phenomena in solids* (Oxford university press, 1960).
[40] W. Li, J. Carrete, N. A. Katcho, and N. Mingo, Computer Physics Communications **185**, 1747 (2014).
[41] M. Omini and A. Sparavigna, Physica B: Condensed Matter **212**, 101 (1995).
[42] L. Lindsay, D. Broido, and T. Reinecke, Physical Review B **87**, 165201 (2013).
[43] P. Giannozzi, J. Phys.: Condens. Matter **21**, 395502 (2009).
[44] J. P. Perdew and A. Zunger, Physical Review B **23**, 5048 (1981).
[45] A. Taylor and R. Jones, Silicon Carbide , 147 (1960).
[46] D. Bimberg, M. Altarelli, and N. Lipari, Solid State Communications **40**, 437 (1981).
[47] M. E. Levinshtein, S. L. Rumyantsev, and M. S. Shur, *Properties of Advanced Semiconductor Materials: GaN, AlN, InN, BN, SiC, SiGe* (John Wiley & Sons, 2001).
[48] J. Serrano, J. Strempfer, M. Cardona, M. Schwoerer-Böhning, H. Requardt, M. Lorenzen, B. Stojetz, P. Pavone, and W. Choyke, Applied physics letters **80**, 4360 (2002).
[49] F. Widulle, T. Ruf, O. Buresch, A. Debernardi, and M. Cardona, Physical review letters **82**, 3089 (1999).
[50] O. Madelung, New Series , 571 (1982).
[51] B. D. Malone and M. L. Cohen, Journal of Physics: Condensed Matter **25**, 105503 (2013).
[52] M. Gmitra and J. Fabian, Physical Review B **94**, 165202 (2016).
[53] A. Lebedev, P. Abramov, E. Bogdanova, S. Lebedev, D. Nel'son, G. Oganesyan, A. Tregubova, and R. Yakimova, Semiconductor Science and Technology **23**, 075004 (2008).
[54] J. Kono, S. Takeyama, H. Yokoi, N. Miura, M. Yamanaka, M. Shinohara, and K. Ikoma, Physical Review B **48**, 10909 (1993).
[55] Q. Song, T.-H. Liu, J. Zhou, Z. Ding, and G. Chen, Materials Today Physics **2**, 69 (2017).
[56] J. Zhou, H. Zhu, T.-H. Liu, Q. Song, R. He, J. Mao, Z. Liu, W. Ren, B. Liao, D. J. Singh, *et al.*, Nature communications **9** (2018).